

STUDY OF A FLUX TRANSFER EVENT WITH CLUSTER SPACECRAFT

P. Robert⁽¹⁾, O. Lecontel⁽¹⁾, A. Roux⁽¹⁾, P. Canu⁽¹⁾, D. Fontaine⁽¹⁾, G. Chanteur⁽¹⁾, J.M. Bosqued⁽²⁾, C. Owen⁽³⁾,
A.N. Fazakerley⁽³⁾, and M.W. Dunlop⁽⁴⁾

⁽¹⁾CETP-IPSL-CNRS, 10-12 avenue de l'Europe, 78140 VÉLIZY-VILLACOUBLAY, FRANCE

⁽²⁾CESR, 9 avenue du Colonel Roche, BP 4346, 31028 TOULOUSE CEDEX 4, FRANCE

⁽³⁾MSSL, UNITED KINGDOM

⁽⁴⁾RAL, UNITED KINGDOM

ABSTRACT

Cluster multipoint measurements are used to study a magnetosheath Flux Transfer Event (FTE), with a typical magnetic signature. A large negative B_y (GSE) component is observed before, during and after the event. Cluster data demonstrate that the FTE is a force free configuration, with a current flowing essentially in the Y (GSE) direction. The current density is filamented, and it shows reversals from parallel to antiparallel to \vec{B} . Energetic electron and ions, escaping from the magnetosphere (antiparallel to \vec{B}), are observed during the magnetic signature of the FTE, as expected. These escaping energetic electrons and ions continue to be observed until 11:33:40; about 2 minutes after the passage of the magnetic structure of the FTE. Surprisingly, during the magnetic signature of the FTE, energetic electrons are also observed in the parallel (to \vec{B}) direction, with fluxes comparable to the antiparallel direction, and larger than in perpendicular direction. These enhanced energetic electron fluxes in parallel and anti-parallel directions indicate that field lines are closed inside the FTE, at least during its early phase (11:30:50-11:31:25 for SC1). During the same time interval the density is about 4 times less than in the adjacent magnetosheath, which is also consistent with being on closed field lines (magnetospheric). At \sim 11:30:50 the 4 S/C cross the magnetopause, a tangential discontinuity (TD), and remain in the closed magnetosphere for about 30 sec. No compelling evidence for a boundary layer (BL) is found during this first crossing. At \sim 11:31:25 the 4 S/C cross a second TD: the boundary between the magnetosphere and a turbulent magnetopause boundary layer (MPBL). From 11:31:25-11:31:50 field lines are alternatively open/closed, as inferred from signatures on energetic electrons. The ion flow velocity is accelerated, at \sim 11:31:50, during the crossing of a third discontinuity; a rotational discontinuity (RD), corresponding to an open magnetopause. While crossing this RD the modulus of the ion flow velocity is multiplied by 2. Thus the acceleration of the ion flow is observed on open field lines, as expected from the standard FTE model (see for instance

Paschmann et al., 1982 [20]). Yet the ion flow velocity is continuous across the second TD, met at 11:31:25, thus the accelerated ion flow is found to penetrate on closed field lines, through a TD, which is unexpected. Our observations demonstrate that the accelerated flow of ions is not limited to open field lines, which indicates that an efficient anomalous transport of the plasma occurs. It is suggested that the anomalous transport, through the inner edge of the MPBL, is due to a fast spatial diffusion associated with large amplitude electromagnetic ULF fluctuations observed simultaneously.

1. INTRODUCTION

The identification of the process(es) that transports the magnetosheath plasma across the dayside magnetopause is a critical issue in magnetospheric physics. Here we restrict our attention to studying transient transport. Russell and Elphic, 1979 [28] have called Flux Transfer Events (FTEs) the transient magnetic signatures observed on ISEE1 and 2, near the magnetopause. A magnetosheath FTE is usually defined as a maximum in the modulus of \vec{B} , together with a bipolar signature on the normal component, in boundary normal coordinates, and a depression in the density (Paschmann et al., 1982 [20]). Energetic ions, from magnetospheric origin, are currently observed in FTEs (Daly et al., 1984 [7]), together with heated magnetosheath plasma. For practical reasons the events that present the characteristics listed above are called magnetosheath FTEs. They are observed by spacecraft initially located in the magnetosheath. There are at least two types of models for FTEs. In the first type of model, FTEs are modelled as twisted open flux tubes linking the magnetosheath to the magnetosphere. Statistics made by Berchem and Russell, 1984 [2] show that FTE generally move northward, while observed in north hemisphere, and southward in the south. These observations suggest that FTEs are formed near the magnetic equator, and correspond to localized reconnection between magnetosheath and magnetospheric flux tubes. In this interpretation the magnetosheath flux tube is cut in two

parts which are connected to their magnetospheric counterparts. Each of the newly connected flux tubes moves essentially poleward. This model implies that FTEs are on open field lines; an important issue for our future discussion; see for instance a review by Paschmann, 1984 [19]. Sibeck, 1990 [31] has proposed a very different model for FTEs. He noticed that localized regions of enhanced pressure are frequently present in the solar wind/magnetosheath. Sibeck showed that the transient response of the outer magnetosphere to these jumps in solar wind dynamic pressure involves a fast-mode compressional wave. If this compressional pulse is faster than the pressure pulse, the magnetopause expands and later retracts. According to Sibeck, this dual response produces a bipolar signature, exactly as for the FTE model described before. The model developed by Sibeck is quite simple; it is based on analogies with fluid mechanics, and does not address an important question: the transport across the magnetopause. Data presented here indicate that the magnetosheath plasma does penetrate on closed field lines.

In the present paper we take advantage of the new diagnosis tools offered by the Cluster tetrahedron, to further analyse FTEs and try to resolve the controversy briefly described above, about their origin. For instance we estimate the current density inside the FTE, from the measurement of the magnetic field vector at the four spacecraft. The corresponding results are compared with the predictions of Saunders et al., 1984 [29], which were based upon dual satellite measurements (ISEE1 and 2).

More generally we use most of the Cluster fields and particle instruments and try to timeline their measurements, at the level of the four spacecraft, to assess directions of propagation. The context and the reasons for choosing the two events discussed here are discussed in section 2. Section 3 is a brief reminder on multi S/C methods. Section 4 describes the fields and particle measurements for the event. Section 5 deals with a comparison between models and data. The conclusions are described in section 6.

2. CONTEXT OF THE EVENT

Figure 1 shows the location of the Cluster tetrahedron in GSE coordinates (2 left panels). Cluster spacecraft (S/C) are moving outward. The orbital plane is located in the afternoon sector; at $\sim 11:30$ UT, the GSE coordinates (in R_E) are approximately (5.72, 8.25, 9.22), for the centre of mass. A map of the magnetic field configuration, deduced from the Tsyganenko 89 model [33], is superimposed. Purple lines correspond to field lines in the noon midnight meridian, while blue and yellow correspond to the projections of the field lines passing by Cluster 4 (C4, in blue) and Cluster1,2,3 (C1,2,3 in yellow). Notice that the field line passing by C4, at the time of the event, is closed, while the three others are open. This indicates that the S/C are close to the magnetopause, as inferred from the Tsyganenko model. The RH panels show the projections of the Cluster tetrahedron, also in GSE. The typical distance between the Cluster S/C is 500-600km.

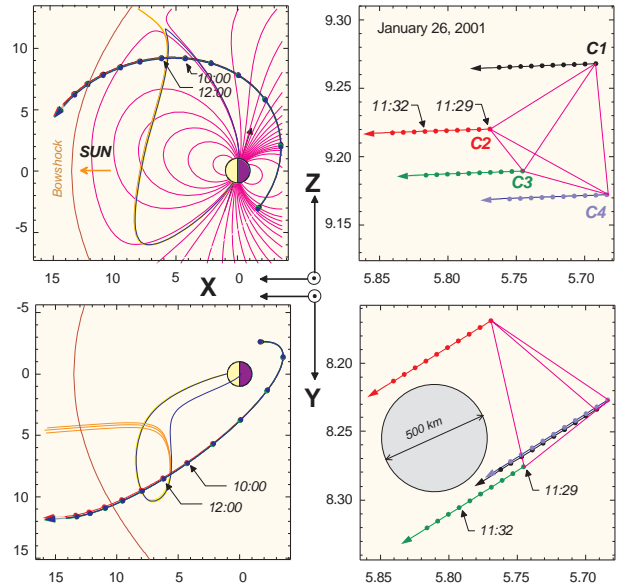


Figure 1. Left: location of CLUSTER spacecraft with respect to the Tsyganenko model. Right: Shape of the tetrahedron.

Notice that Cluster 4 (C4 afterwards) is closer from the Earth than its companions, which explains why the Tsyganenko field line passing by C4 is closed, while the others are open.

Figure 2 is a composite showing more than 2 hours of 4 second resolution data from the fluxgate magnetometer (FGM) and a frequency-time spectrogram from the search coil magnetometer (SCM). For a description of these instruments see Balogh et al., 1997 [1] and Cornilleau et al., 1997 [6]. Minimum variance analysis (MVA) has been applied to FGM data; the elements of the rotation matrix are given on the figure, together with the values of λ that characterize the ellipsoid of variance. The 3 values of λ are quite different, hence the proper axis of the ellipsoid are well defined, and the results of the MVA are significant. The large amplitude fluctuations observed in particular on B_L , before 11:10, correspond to multiple crossings of the magnetopause. After 11:20 Cluster S/C remain in the magnetosheath, except maybe during the short lasting isolated events, at $\sim 11:31$, 12:10, and possibly at 12:02. In the rest of the paper we will focus on the first event observed at $\sim 11:31$. Unlike magnetopause crossings that occurred around 11:00, these events show a large increase in the modulus of \vec{B} and a bipolar signatures in B_N , as expected for a magnetosheath FTE.

3. REMINDER ON MULTI S/C METHODS

3.1. Reminder on $Curl(\vec{B})$ computation

Two classical methods are now well known ; the curlometer (Dunlop 1990 [10]), and the barycentric coordinate (Chanteur 1993 [5]). The first one computes the circulation of \vec{B} on each face of the tetrahedron formed by the 4 S/C, and obtain the current density via the ampere law

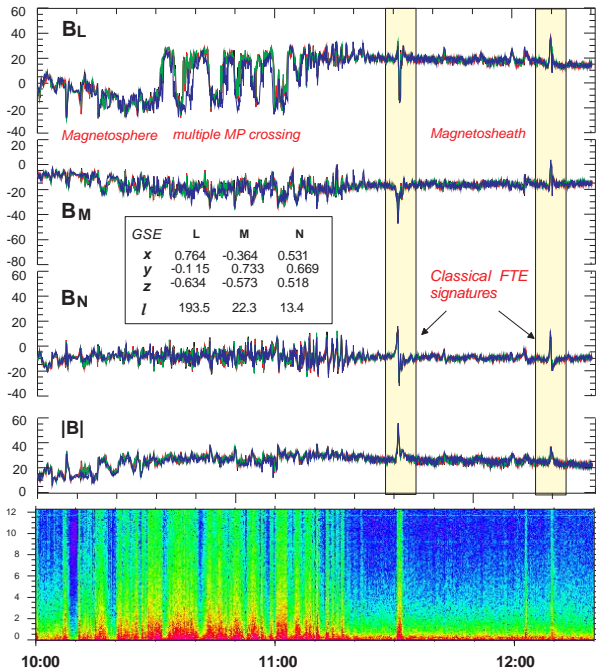


Figure 2. Identification of the FTE by its magnetic signature.

$\mu_0 \vec{J} = \int \vec{B} \cdot d\vec{l}$ applied on each face. Then, the 4 results are combined to estimate the global current \vec{J} . The second one gives directly the gradient matrix: the diagonal terms give the divergence of \vec{B} , while the non-diagonal terms give the curl of \vec{B} . It has been shown [22] that the two methods are mathematically equivalent and lead to the same results. It must be kept in mind that the two methods assume the linearity of \vec{B} inside the tetrahedron. On the other hand, in order to use data and time from 4 S/C, sampled at the same frequency but not at the same time, data has to be resampled and time aligned.

Several studies [10], [23] investigate various source of errors, and their effect upon the accuracy of \vec{J} [9], [11], [24], [26], [25], [22]. The influence of the shape of the tetrahedron, defined by the Elongation and Planarity parameters [27], on the accuracy of the estimate of \vec{J} , has been discussed in Robert et al, 1998 [22].

3.2. Reminder on discontinuity analysis method

Discontinuity analysis method was developed by Mottez and Chanteur, 1994, [18], and extended by Dunlop, 1998 [12], Chanteur, 1998 [3], [4] and Schwartz, 1998 [30]. The method used here comes from a code source delivered by G. Chanteur (private communication), assuming the crossing by the 4 Cluster S/C of a planar discontinuity. The program give the normal direction to the discontinuity plane, as well as the velocity of the discontinuity in the normal direction.

4. DETAILED ANALYSIS

4.1. Fields and currents

The top panels (a,b,c,d) of figure 3 shows full resolution data from the tri-axis Flux-Gate Magnetometer (FGM) on Cluster. Magnetic field data are plotted in boundary normal coordinates obtained by applying Minimum Variance Analysis (MVA) to the period covered by figure 2. Again we see the typical signature of a FTE, with a bi-modal signature \pm on B_N , and an increase in the modulus of \vec{B} by almost a factor 2, reaching 55nT at 11:31:10. This maximum occurs during the early phase of the event, but large amplitude variations in the direction of \vec{B} still occur later; for instance the B_L component decreases (~ 20 nT) at $\sim 11:31:25$ and increases (~ 40 nT) at 11:31:50. These large and rapid variations in the components correspond to rotations of the magnetic field, with little variations of the modulus of \vec{B} . This suggests that the FTE signature can be split in two periods labelled B and C in figure 3: first a compression (B), and later two rotations (C).

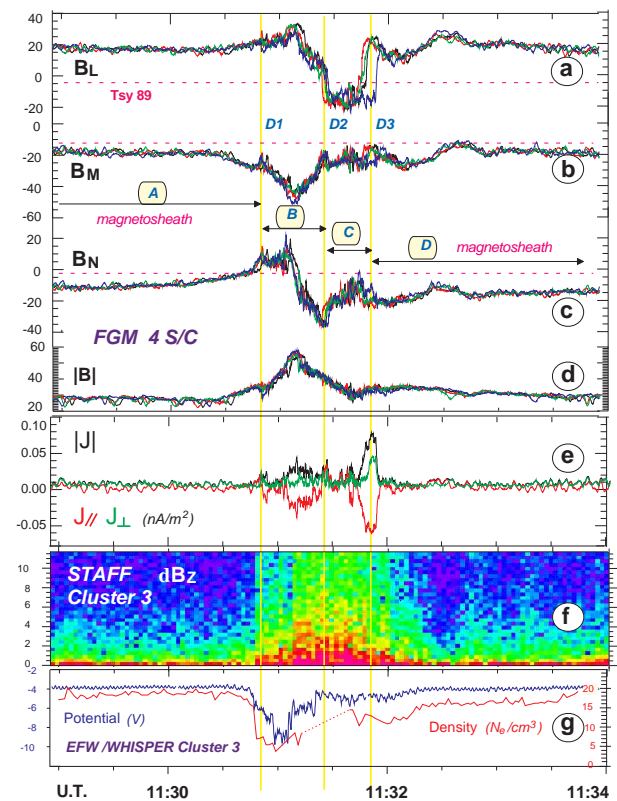


Figure 3. Zoom on FTE period. The 3 discontinuities D1, D2, D3 separating different regions of space are shown in yellow.

The distance between Cluster S/C is of the order of 500-600 km, then the current density can be estimated (Dunlop et al, 1990 [10], Chanteur, 1998 [3], [4], Robert et al., 1998, [22]) inside structures with a typical size $L > 500$ -600 km. The typical transverse size of the FTEs is $2 R_E$, hence the estimate of $curl(\vec{B})$ is a priori valid. The current density computed from the barycentric method

(Chanteur 1993 [5]) is shown in panel e. In agreement with the prediction of Saunders et al., 1984, [29]) we find a relatively large current density inside the structure: $J_{max} \approx 25 \text{ nA/m}^2$, around 11:31:10. The current density, is essentially antiparallel to \vec{B} (red curve on panel e), mostly in the Y (GSE)/azimuthal direction (toward the evening sector). An even larger (negative) peak in \vec{J} is found at $\sim 11:31:50$. However the linear approximation, used to compute $\text{curl}(\vec{B})$, is not valid during this period, because the values of B_L at the various S/C (S/C4 especially) are very different; the relative variation is too large ($\sim 100\%$ or more). Another approach, adapted to sharp gradients, will be discussed and used in section 5 to estimate the current density.

A dynamical spectrum of magnetic fluctuations measured from STAFF (Cornilleau et al., 1997 [6]) is shown in figure 3, panel f. The level of the fluctuations and their frequency bandwidth are largely enhanced during the FTE. The amplitude (not shown) is a few nT. The last panel (panel g) gives the density, estimated (whenever possible) from the relaxation sounder WHISPER (Décrou et al, 1997 [8]). This density profile is consistent with the density profile deduced from the potential (V) measured by EFW (Gustafsson et al, 1997 [13]). The vertical yellow lines labelled D1,2,3 correspond to crossings of discontinuities. D2 and D3 correspond to sharp variations in B_L . D1 corresponds to a smaller magnetic field variations, a decrease in the density, and a sudden change in the energy spectrum of electrons, as shown in figure 5. During periods A and D the density is $\sim 20/\text{cm}^3$, as expected for the magnetosheath. During period B a large density drop down to $\sim 5/\text{cm}^3$ is observed, together with an increase in the modulus of \vec{B} , and a positive excursion of B_N .

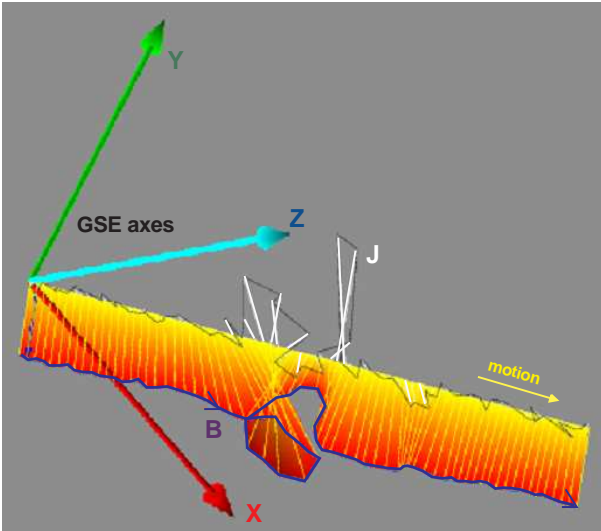


Figure 4. 3-D view of \vec{B} and \vec{J} along trajectory, showing relationship between the rotation of \vec{B} and large currents (\vec{J}).

Figure 4 shows a 3-D representation of the magnetic field vector, in GSE coordinates: X(red), Y(blue), Z(green), as

plotted along the direction of the motion of the structure (the S/C are essentially fixed). This plot shows again the increase of $|\vec{B}|$, followed by two rotations. Current density, \vec{J} (in white), is superimposed. When \vec{J} is large, it tends to be antiparallel to \vec{B} .

4.2. Particle measurements

4.2.1. Ions from CIS

The 3 top panels of figure 5 show data, from CIS (Reme, 1997 [21]) on C1, plotted in GSE coordinates. Data from C3 and C4 are very similar. The 3 components of the velocity are displayed on panel a. In the magnetosheath the largest component of the velocity is $V_x \sim 140 \text{ km/sec}$, while $V_y \sim 40 \text{ km/sec}$, and $V_z \sim 100 \text{ km/sec}$. During crossing of the FTE, V_x and V_z are essentially multiplied by 2; we get $V_{xmax} \sim 350 \text{ km/sec}$, $V_{zmax} \sim 200 \text{ km/sec}$. Panel c shows the ion flux versus energy and time. Before and after the FTE crossing (periods A and E), the S/C is in the magnetosheath; as indicated by the large flux at energies below 1keV.

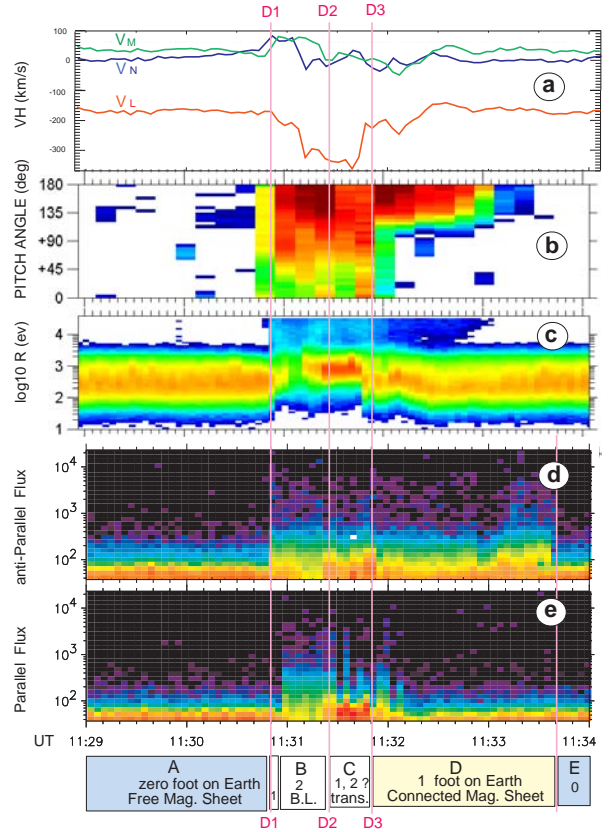


Figure 5. Particles data: identification of regions and boundaries.

During the crossing of the FTE (periods B and C), the count rate at low energies (below a few hundred eV's) decreases, but a fraction of the magnetosheath plasma is heated or accelerated from a few hundred eV, in the magnetosheath, to about 1 keV. The flow velocity (top panel)

being ~ 300 km/sec (which corresponds to 1 keV), we conclude that the ions are accelerated rather than heated. In addition to this accelerated ion population, presumably coming from the magnetosheath, energetic ions, which were absent in the magnetosheath, show up when the FTE begins to be observed (at $\sim 11:30:50$), and continue to be observed till $\sim 11:33:00$. These energetic ions have to come from the magnetosphere. This is confirmed by panel b where the flux of energetic ions (6.7-28 keV) is plotted versus pitch angle (PA). During the magnetic signature of the FTE (periods B and C) the flux is larger for $\sim 180^\circ$ PA, but still substantial for $PA < 90^\circ$. After 11:31:50 (period D) large energetic ion fluxes are found only for $PA > 90^\circ$, as expected for energetic ions moving away from the magnetosphere, along open field lines. We notice that these energetic ions are observed for about 3 mn.; three times the duration of the magnetic signature of the FTE.

4.2.2. Electrons from PEACE

Figure 5 shows the electron flux, from the electron spectrometer, PEACE (Johnstone et al., 1997 [15]), in directions antiparallel (panel d) and parallel to \vec{B} (panel e), for S/C1. There are almost no electrons beyond a few hundred eV in region A and E (before $\sim 11:30:50$ and after 11:33:40); regions A and E correspond to the free magnetosheath, with no magnetic footprint on Earth. A sudden increase in the electron flux above a few 1 keV is observed at 11:30:48 for the antiparallel flux, and at 11:30:56, for the parallel one, while the magnetic signature of the FTE develops. This sudden increase in the energy range corresponds to D1. After this enhancement the flux of energetic electrons (say above 1 keV) is typical of the magnetosphere. Enhanced fluxes of antiparallel energetic electrons are observed till $\sim 11:33:40$. For parallel energetic electrons, enhanced fluxes last up to $\sim 11:31:25$ (region B), followed by short lasting burst between $\sim 11:31:25$ and $\sim 11:32:00$. The observation of equivalent parallel and antiparallel fluxes of energetic electrons indicates that the field line, in region B at least, are closed (two footprints on Earth). Furthermore the distribution functions, in region B (not shown) are anisotropic, with number densities in parallel and antiparallel directions larger than in the perpendicular direction. Such a situation cannot develop on open field lines. Between 11:31:50 and 11:33:40 (region D) field lines are open (one footprint on Earth). Region C is more complex; energetic antiparallel electrons are regularly observed, while energetic parallel electrons are alternatively present. Furthermore the bursts of energetic parallel electrons differ on different spacecraft; parallel energetic electrons cover the whole period C, on S/C4, the closest from the Earth. This is consistent with being in the magnetopause boundary layer.

5. DISCUSSION

We use Cluster data to test models. In particular advantage is taken of the good time resolution of particle instruments, and of the spatial resolution associated with multipoint measurements; for instance discontinuity analysis

and curlometer.

5.1. Discontinuity analysis

For the three discontinuities (D1, D2, D3) the magnetic fields components, at the various S/C, have similar time profiles, once a time shift is applied. We can assume quasi-stationarity during the crossings of these discontinuities. Knowing the locations of the 4 S/C, and the time of the crossings of the discontinuities by each S/C, we can calculate the direction of the normal to the discontinuity and the velocity along this normal. The method is discussed in section 3.2.

Discontinuities	D1	D2	D3
	$\sim 11:30:50$	$\sim 11:31:25$	$\sim 11:31:50$
V_{Dn} LMN (km/s)	169	196	68
V_p LMN (km/s)	-180,48,70	-331,0,-15	-285,10,7
B_n (nT)	-4	4	4
$W_{Pn} = V_{Pn} - V_{Dn}$ (km/s)	-13	7	12
W_{Pn}/V_{Dn} (%)	8	4	18
ΔB_t (nT)	16, 4, 0	-3, 23, 2	0, -44, 2
ΔV_t (km/sec)	20, 64, -8	-8, 6, 4	15, -156, -5

Table 1. Characterization of the discontinuities. Tests of jump conditions.

Table 1 gives the velocity of the discontinuity along its normal (V_{Dn}), and the plasma velocity, V_p (in LMN). B_n , and V_{Pn} are the projections along the normal in the discontinuity frame. We note that $W_{Pn}/|V_{Dn}|$ is quite small; less than 10% for D1 and D2, which is certainly within error margins. Then the low energy ions move essentially with the discontinuities, at least for D1 and D2, which suggests that they are tangential discontinuities (TD). For D3 V_{Pn} is also relatively small, but the ratio $W_{Pn}/|V_{Dn}|$ is larger (18%). For a TD B_n should be null. Table 1 shows that B_n is indeed small. The third test is the relation between the jumps in the velocity and in the magnetic field components parallel to the discontinuity (ΔV_t and ΔB_t). For D1 ΔV_t and ΔB_t are not parallel. The same is true for D2; D1 and D2 can not be RT. Conversely, table 1 shows that for D3 (i) ΔV_t and ΔB_t are essentially parallel, and (ii) $\{\Delta V_t\} = 157$ km/sec $\sim \{\Delta B_t\}/\sqrt{(2\mu_0 N M_i)} = 153$ km/sec., for $N \sim 20$ p/cm³. Thus D3 is a RD, while D1 and D2 are TD's. Notice that the normal to D1 and D2 have very different directions; D1 moves essentially along Z (GSE), while D2 moves along -X (GSE).

5.2. Nature of the discontinuities

Particle measurements have been used to establish the mapping of the field lines. The lowermost part of figure 5 shows the result of this analysis; it can be used to identify the nature of the discontinuities. D1 corresponds to a relatively smooth magnetopause (MP)/inner

boundary of magnetopause boundary layer (MPBL). Indeed it is not clear that there is a boundary layer (BL) during the first crossing. Electron data suggest that there is only one magnetic footprint on Earth for a short period (2spin) between 11:30:48 and 11:30:56 (on SC1), which might correspond to a MPBL. Yet magnetic data do not indicate the existence of two separate boundaries. In any case D1, the boundary (between open and closed field lines), is a TD. D2 is a sharp magnetic discontinuity, interpreted as the inner boundary of the magnetopause boundary layer (MPBL). It is also a TD. D3 corresponds to a sharp change in magnetic field direction. It is a RD, interpreted as an open magnetopause.

5.3. Current density inside FTEs

5.3.1. Large scale structure

Originally Russell and Elphic, 1979, [28] attributed the magnetic signature of FTEs to a draping of the magnetosheath magnetic field around a tubular structure. In this "fluid" picture the magnetic field is frozen in the plasma everywhere but in a very small diffusion region, which is likely to be close to the equator, and is unlikely to be crossed by the spacecraft; especially by polar orbiting satellites such as Cluster. Saunders et al, 1984 [29] adopted a different perspective; they suggested that the torsion of the field line is due to a line-current circulating inside the FTE. Various hypothesis regarding the closure of this current were considered by Lee, 1986 [16] and by Southwood, 1987 [32]. Figure 4.1 shows the current density deduced from $\text{curl}(\vec{B})$; the estimate via $\text{curl}(\vec{B})$ is valid before 11:31:25. As pointed out in section 3.1. we find $J \sim 25 \text{ nA/m}^2$ in region B, between D1 and D2, with \vec{J} along the Y direction; essentially antiparallel to \vec{B} . The current density can also be estimated by assuming that a quasi-steady and homogeneous current density tube is passing by the S/C. the method is discussed by Robert et al, 1998 [22]. For $R \sim 1R_E$ (radius of current tube) and $\delta B \sim 30\text{nT}$, we get $J \sim 2\delta B / \mu_0 R \sim 10\text{nA/m}^2$. The comparison between these values suggests that current density is not homogeneous. Indeed the current density estimated via $\text{curl}(\vec{B})$, varies along the trajectory. The scale of the current density variation is even smaller for discontinuities, thus the curlometer method cannot be used, as discussed below.

5.3.2. Current density within discontinuities

The jumps observed in the magnetic components; principally on B_N , for D1 and on B_L for D2 and D3, correspond to large currents with spatial scales smaller than the distance between the S/C; the current density cannot be calculated via a linear estimator (see discussion in section 3.1). The normal velocities, V_{Dn} corresponding to D1, D2, and D3 are given in table 1. The thickness of the current sheet is given by $e = V_{Dn} \delta t$, where δt is the typical duration of the crossing of this discontinuity by each Cluster S/C. For D1 we get $\delta t \sim 8\text{sec}$ and $V_{Dn} = 169\text{km/sec}$, thus $e \sim 1350\text{km}$, and $J \sim 10\text{nA/m}^2$. For D2, $\delta t \sim 1\text{sec.}$, $V_{Dn} = 196\text{km/sec.}$, hence $e \sim 196\text{km}$ and $J \sim 100\text{nA/m}^2$, while for D3, $\delta t \sim 3\text{sec}$, $V_{Dn} = 68\text{km/sec.}$,

$e = 204\text{km}$, and therefore $J = 180\text{nA/m}^2$. For D2 and D3 B_L is the dominant component, hence the currents are essentially perpendicular to the L direction. B_M being the smallest component, the largest component of \vec{J} is along the M direction; essentially antiparallel to \vec{B} . Notice that the modulus of the current associated with D2 and D3 is almost one order of magnitude larger than the current determined from the curlometer. The scales of these currents being smaller than the distance between the S/C this is to be expected. The direction of the current, however, seems to be well estimated by the curlometer technic.

5.3.3. FTEs are force free

In summary we measure large scale field aligned current density structures inside FTEs (period B) as well as small scale current density structures. In both cases the current is parallel or antiparallel to \vec{B} . Hence \vec{J} is force free. Inside FTEs the current density is not homogeneous; it is highly filamented.

5.4. Spatial structure of the FTE

Discontinuity analysis has been used to infer the nature and the motion of the boundaries. The corresponding velocities are given in table 1 and displayed in Figure 6, which is an attempt to put together all the observational features, from fields and particle measurements. It should not be considered as a model, but just as a mean of displaying the available information. Figure 6 shows the projections of the magnetic field (\vec{B} , in yellow) and ion velocity (\vec{V} , in green) onto the LN plane. For clarity \vec{B} and \vec{V} are plotted along different lines. Plasma density is indicated by color coded circles. Thin lines (full and dotted) give possible extrapolations of \vec{B} ; they are also color coded to indicate the number of footprint on Earth (green for 0, blue for 1, brown for 1 or 2, and red for 2). The red arrows stand for the normal velocity to the three discontinuities. Thick dashed lines are extrapolations of the MP and of the inner boundary of the MPBL. The shape of the structure is drawn in a frame moving with the structure, which is assumed to be stationary in that frame (see a discussion in section 5.5). Then the S/C are moving with respect to the structure; their relative motion is along the L-axis. C1 is the last to cross the structure.

In that frame the 4 S/C move from the free magnetosheath (top of figure 6) to the magnetosphere, crossing D1 (MP/inner boundary of MPBL) at $\sim 11:30:50$; the S/C are now on closed field lines. From 11:30:40, to $\sim 11:31:10$, $V_N > 0$; the magnetopause expands. This is consistent with the outward motion of D1. On the other hand, from 11:31:10 to 11:31:25, $V_N < 0$ and D2 moves inward. Given that there is a large maximum in $|\vec{B}|$ (55nT) at $\sim 11:31:10$, this forth and back MP motion can be interpreted as the passage of a magnetic pressure pulse, as suggested by Sibeck, 1990 [31]. At $\sim 11:31:25$ the spacecraft move across D2, a TD corresponding to the inner edge of the MPBL and remains in the MPBL till 11:31:50. The MPBL is a turbulent layer, with large amplitude magnetic fluctuations $\delta B/B \sim 10\text{-}20\%$; field

lines are generally open with one footprint on the Earth. The magnetopause proper is crossed at $\sim 11:31:50$. It is a RT; field lines connect the magnetosphere to the magnetosheath. Only after $\sim 11:33:40$ is the free magnetosheath met again. Notice that all along this period the direction of \vec{V} was almost constant, while its modulus was multiplied by 2 as the flow crossed D3 (MP).

5.5. Interpretation

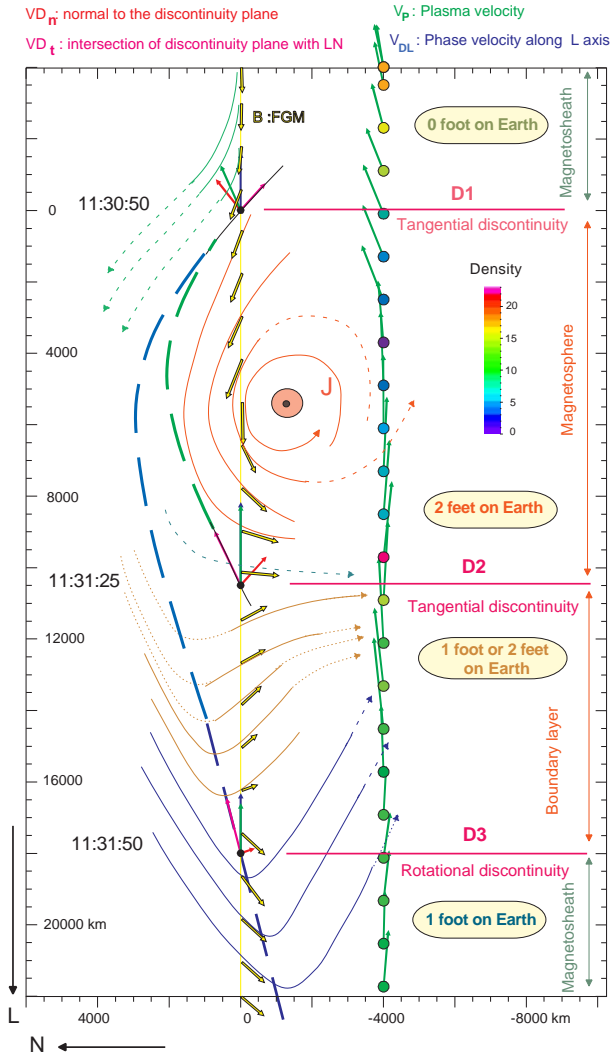


Figure 6. Suggestion of a model based on propagation of a bulge along L.

5.5.1. Comparison with models

As discussed in the introduction, and in a recent review paper by Lui, 2001 [17], there are essentially two models for describing the magnetic signatures of what is usually called a FTE. As mentioned above V_N , which is null outside the FTE, oscillates inside it. The oscillations of V_N are essentially in phase with B_N . Given that we observe oscillations on both B_N and V_N , it seems appropri-

ate to interpret them as boundary oscillations. In Sibeck's model the early signature of the transient interaction between a dynamic pressure pulse and the magnetopause is a magnetic pressure pulse carried by a fast wave. The motion along the MP of this pulse leads to an expansion, followed by a retraction of MP. This is consistent with our observations; we indeed observe a large increase in $|\vec{B}|$, from 25 to 55nT (phases A&B) and a bipolar signature in V_N and B_N . Sibeck's model, however, does not describe the acceleration of the flow.

The most often quoted FTE model is based on a change of magnetic topology, associated with magnetic reconnection. In this model the FTE is a newly open flux tube, presumably in the near equatorial region, moving poleward. Acceleration occurs on open field lines. As discussed in subsection 5.1 the abrupt acceleration of the ion flow observed around 11:31:50 (D3) does correspond to the change (rotation) in \vec{B} as the RD (the MP) is crossed. This is consistent with the standard FTE model. The penetration of the accelerated ion flow on closed field lines, however, is not addressed by this model. Our observations, summarized in figure 6, demonstrate that the accelerated ion flow does penetrate inside the magnetosphere proper (i.e. on closed field lines), which is not explained by the two models discussed above. How can this be interpreted?

5.5.2. Penetration of magnetosheath plasma on closed field lines

Close inspection of figure 5c shows that accelerated ions are penetrating inside closed field lines. Penetration of accelerated magnetosheath ions can be driven by spatial diffusion associated with fluctuations. Figure 3f does give evidence for enhanced magnetic fluctuations between D1 and D3. The amplitude reaches ~ 5 nT. The maximum diffusion, at Bohm rate, for $\rho_i \sim 100$ km (for 1keV ions in a 30nT field) is $D = \rho_i^2 / \Omega_{H^+} \sim 3.10^9 m^2.s$; accelerated ions diffuse through D2 (196km, see section 5.3) in 12 sec. Assuming that the waves are kinetic Alfvén waves, we get $D = (\pi/2)(V_A)^2(\delta B/B)^2/(V_{res}\Delta k//)$ (adapted from Hasegawa and Mima, 1978 [14]). For $F \sim F_{H^+}/2 \sim 0.25$ Hz ($F_{H^+} \sim 0.5$ Hz for 30nT), $\delta B/B \sim 1/5$, $N \sim 20/cm^3$ and $V_{res}\Delta k// \sim \omega$, we get $D \sim 10^9$. With this diffusion coefficient D2 is crossed in ~ 40 sec. Then, diffusion can be a viable explanation. The range of ion penetration varies as the square root of time. How long can it last?

So far we have not discussed an important point: the velocity of the structure is quite different at the leading and trailing edges: -180km/sec and -330km/sec at D1 and D2, respectively, which implies a very fast deformation and a breaking of the structure over a time ~ 50 sec. Then the structure is unlikely to live much more than 50sec. The persistence of escaping electrons and ions up to 11:33:40, however, suggests that the life time of the structure is longer (≥ 180 sec).

Whatever the process we note that the penetration of accelerated ions on closed field lines is a two step process,

(i) ions are accelerated on open field lines at a RD (D3), behind the travelling magnetic pressure pulse, and (ii) they penetrate, through the trailing edge of this pressure pulse (D2), on closed field lines.

6. CONCLUSIONS

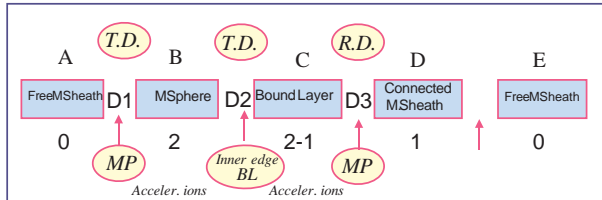


Figure 7. Schematic diagram summarizing the event

We have presented a multi instrument, multi satellite study of a magnetosheath FTE, characterized by a large increase in the modulus of \vec{B} , a bi-polar signature on B_N , and a decrease in the density. During the whole period a large negative B_y (GSE) component is observed, in the magnetosheath as well as during the short lasting (~ 30 sec) penetration in the magnetosphere. Given the location of the S/C in the early afternoon sector, a negative B_y is to be expected. Cluster data demonstrate that the FTE is a force free magnetic structure, with a current flowing essentially in the Y (GSE) direction. The current density is filamented and shows reversals from parallel to antiparallel to \vec{B} . In the MVA frame the normal components (V_N and B_N) which are almost null outside the FTE, take positive and later negative values during the FTE. This signature can be interpreted as an expansion, followed by a retraction of the magnetopause, in response to an approaching magnetic pressure pulse, as in Sibeck's model, 1990 [31]. Sibeck, however, did not consider the penetration of the plasma in the magnetosphere. Data presented here indicate that the magnetosheath plasma is accelerated on open field lines (as in the standard FTE model), and penetrates on closed magnetospheric field lines, during the FTE. Fields and particles signatures give evidence for the crossings of 3 sharp discontinuities. D1 ($\sim 11:30:50$), is a TD, it corresponds to the inbound crossing of the magnetopause (MP). During this first crossing the boundary layer (BL), is too thin to be analysed. D2 ($\sim 11:31:25$) is also a TD; it corresponds to the transition between closed magnetospheric field lines and the inner boundary of the MPBL, which is now relatively thick (~ 600 km; the distance between the S/C). D3 (11:31:50) is a RD, corresponding to the magnetopause; it is crossed outbound. The ion flow velocity is accelerated through D3; in agreement with the standard FTE model. Then the flow velocity is accelerated at the trailing edge of the FTE and it overtakes the magnetic structure, between D3 and D2. D2 being a TD no net ion flow is to be expected through it. Yet the ion flow velocity is continuous across D2. The continuity of the ion flow across D2 suggests that the plasma penetrates through D2 (onto closed field lines) via an anomalous process such as fast spatial diffusion associated with ULF fluctuations. The large

amplitude electromagnetic ULF fluctuations (~ 5 nT) observed simultaneously can produce the requested anomalous transport across the thin current sheet D2 (~ 200 km thick).

A simple cartoon can be proposed to help visualize present results: the magnetic pressure pulse, as it propagates along the MP acts as a zipper; it leaves behind it opened field lines. Then the opening of the field lines is not limited to a remote reconnection site (e.g. equatorial); it occurs all along the motion of the zipper. Further work is underway to investigate other FTEs and decide upon the generality of the above results.

REFERENCES

1. A. Balogh, M.W. Dunlop, S.W. H. Cowley, D.J. Southwood, J.G. Thomlinson, K.-H. Glassmeier, G. Musmann, H. Luhr, S. Buchert, M.H. Acuna, D.H. Fairfield, J.A. Slavin, W. Riedler, K. Schwingschuh, and M.G. Kivelson. The Cluster magnetic field investigation. *Space Science Reviews*, 79:65–91, 1997.
2. J. Berchem and C.T. Russel. Flux Transfer Events on the magnetopause: spatial distribution and controlling factors. *J. Geophys. Res.*, 89:689–703, 1984.
3. G. Chanteur. Spatial interpolation for four spacecraft: Theory. In G. Paschman and P. Daly, editors, *Analysis Methods for Multi-Spacecraft Data*, ISSI Scientific Report SR-001, chapter 14, pages 349–369. European Space Agency, July 1998.
4. G. Chanteur and C.C. Harvey. Spatial interpolation for four spacecraft: Application to magnetic gradients. In G. Paschman and P. Daly, editors, *Analysis Methods for Multi-Spacecraft Data*, ISSI Scientific Report SR-001, chapter 15, pages 371–393. European Space Agency, July 1998.
5. G. Chanteur and F. Mottez. Geometrical tools for Cluster data analysis. In *Proc. International Conf. "Spatio-Temporal Analysis for Resolving plasma Turbulence (START)"*, Aussois, 31 Jan. 31–5 Feb. 1993, ESA WPP-047, pages 341–344. European Space Agency, Paris, France, 1993.
6. N. Cornilleau-Wehrlin, P. Chauveau, S. Louis, A. Meyer, J.M. Nappa, S. Perraut, L. Rezeau, P. Robert, A. Roux, C. de Villedary, Y. de Conchy, L. Friel, C.C. Harvey, D. Hubert, C. Lacombe, R. Manning, F. Wouters, F. Lefeuvre, M. Parrot, J.L. Pinçon, B. Poirier, W. Kofman, and P. Louarn. The CLUSTER spatio-temporal analysis of field fluctuations (STAFF) experiment. *Space Science Reviews*, 79:107–136, January 1997.
7. P.W. Daly, T.R. Sanderson, and K.-P. Wenzel. Survey of energetic ($E > 35$ keV) ion anisotropies in the deep geomagnetic tail. *J. Geophys. Res.*, 89:10,733–10,739, 1984.
8. P.M. Décréau, P.Fergeau, V. Krasnoselskikh, M. Lévêque, P. Martin, O. Randriamboarison, F.X. Sené, J.G. Trotignon, P. Canu, and P.B. Mogensen. WHISPER, a resonance sounder and wave analyser: performances and perspectives for the CLUSTER mission. *Space Science Reviews*, 79:157–193, January 1997.
9. M.W. Dunlop and A. Balogh. On the analysis and interpretation of four spacecraft magnetic field measurements in terms of small scale plasma processes. In *Proc. International Conf. "Spatio-Temporal Analysis for Resolving plasma Turbulence (START)"*, Aussois, 31 Jan. 31–5 Feb. 1993, ESA WPP-047, pages 223–228. European Space Agency, Paris, France, 1993.
10. M.W. Dunlop, A. Balogh, D.J. Southwood, R. C. Elphic, K.-H. Glassmeier, and F. M. Neubauer. Configurational sensitivity of multipoint magnetic field measurements. In E.J. Rolfe, editor, *Proceedings of the International Workshop on "Space Plasma Physics Investigations by Cluster and Regatta"*, Graz, Feb. 20–22, 1990, ESA SP-306, pages 20–22. European Space Agency, Paris, France, May 1990.

11. M.W. Dunlop, D.J. Southwood, and A. Balogh. The Cluster configuration and the directional dependence of coherence lengths in the magnetosheath. In *Proc. International Conf. "Spatio-Temporal Analysis for Resolving plasma Turbulence (START)"*, Aussois, 31 Jan. 31–5 Feb. 1993, ESA WPP-047, pages 295–299. European Space Agency, Paris, France, 1993.
12. M.W. Dunlop and T.I. Woodward. Multi-spacecraft discontinuity analysis: Orientation and motion. In G. Paschman and P. Daly, editors, *Analysis Methods for Multi-Spacecraft Data*, ISSI Scientific Report SR-001, chapter 11, pages 271–305. European Space Agency, July 1998.
13. G. Gustafsson and R. Boström and G. Holmgren and A. Lundgren and K. Stasiewicz. and L. Åhlén and F.S. Mozer and D. Pankow and P. Harvey and P. Berg and R. Ulrich and A. Pedersen and R. Schmidt and A. Butler and A.W.C. Fransen and D. Klinge and M. Thomsen and C-G. Fälthammar and P-A. Lindqvist and S. Christensson and J. Holtet and B. Lybekk and T.A. Sten and P. Tanskanen and K. Lappalainen and J. Wygant. Hybrid simulation codes with application to shocks and upstream waves. *Space Science Reviews*, 42:53–67, 1985.
14. A. Hasegawa and K. Mima. Anomalous transport produced by Kinetic Alfvén turbulence. *J. Geophys. Res.*, 83(A3):1117–1127, 1978.
15. A.D. Johnstone, C. Alsop, S. Burge, P.J. Carter, A.J. Coates, A.J. Coker, A.N. Fazakerley, M. Grande, R.A. Gowen, C. Gurgiolo, B.K. Hancock, B. Narheim, A. Preece, P.H. Sheather, J.D. Winningham, and R.D. Woodliffe. PEACE: A plasma electron and current experiment. *Space Science Reviews*, 79:351–398, 1997.
16. L.C. Lee. Magnetic flux transfer at the earth's magnetopause, in solar wind magnetosphere coupling. pages 297–314. Terra Sc., Tokyo, 1986.
17. A.T. Lui. Current controversies in magnetospheric physics. *Rev. Geophys.*, 39:535–563, 2001.
18. F. Mottez and G. Chanteur. Surface crossing by a group of satellites: a theoretical study. *J. Geophys. Res.*, 99:13499–13507, 1994.
19. G. Paschmann. The Earth's Magnetopause, Achievement of the IMS. ESA SP-217, page 0. European Space Agency, 1984.
20. G. Paschmann, G. Haerendel, I. Papamastorakis N. Sckopke, S.J. Bame, J.T. Gosling, and C.T. Russel. Plasma and magnetic field characteristics of magnetic flux transfer events. *J. Geophys. Res.*, 87:2159, 1982.
21. H. Rème, J.M. Bosqued, J.A. Sauvaud, A. Cros, J. Dandouras, C. Aoustin, C. Martz, J.L. Médale, J. Rouzaud, E. Möbius, K. Crocker, M. Granoff, L.M. Kistler, D. Hovestadt, B. Klecker, G. Paschmann, M. Ertl, E. Künneth, C.W. Carlson, D.W. Curtis, R.P. Lin, J.P. McFadden, J. Croyle, V. Formisano, M. DiLellis, R. Bruno, M.B. Bavassano-Cattaneo, B. Baldetti, G. Chionchio, E.G. Shelley, A.G. Ghielmetti, W. Lennartson, A. Korth, H. Rosenbauer, I. Szemerey, R. Lundin, S. Olson, G.K. Parks, M.Mc. Carthy, and H. Balsiger. The CLUSTER Ion Spectrometry Experiment. *Space Science Reviews*, 79:303, 1997.
22. P. Robert, M.W. Dunlop, A. Roux, and G. Chanteur. Accuracy of current density determination. In G. Paschman and P. Daly, editors, *Analysis Methods for Multi-Spacecraft Data*, ISSI Scientific Report SR-001, chapter 16, pages 395–418. European Space Agency, July 1998.
23. P. Robert and A. Roux. Accuracy of the estimate of J via multi-point measurements. In E.J. Rolfe, editor, *Proceedings of the International Workshop on "Space Plasma Physics Investigations by Cluster and Regatta"*, Graz, Feb. 20–22, 1990, ESA SP-306, pages 29–35. European Space Agency, Paris, France, may 1990.
24. P. Robert and A. Roux. Influence of the shape of the tetrahedron on the accuracy of the estimation of the current density. In *Proc. International Conf. "Spatio-Temporal Analysis for Resolving plasma Turbulence (START)"*, Aussois, 31 Jan. 31–5 Feb. 1993, ESA WPP-047, pages 289–293. European Space Agency, Paris, France, 1993.
25. P. Robert, A. Roux, and G. Chanteur. Accuracy of the determination of the current density via four satellites. In *Abstracts*, Boulder, Colorado, July 1995. International Union of Geodesy and Geophysics, XXI General Assembly. Presentation GAB51H-06.
26. P. Robert, A. Roux, and O. Coeur-Joly. Validity of the estimate of the current density along Cluster orbit with simulated magnetic data. In *Proceedings of Cluster Workshops, Braunschweig*, 28–30 Sep. 1994, Toulouse, 16–17 Nov. 1994, ESA SP-371, pages 229–233. European Space Agency, Paris, France, June 1995.
27. P. Robert, A. Roux, C.C. Harvey, M.W. Dunlop, P. Daly, and K-H. Glassmeier. Tetrahedron geometric factors. In G. Paschman and P. Daly, editors, *Analysis Methods for Multi-Spacecraft Data*, ISSI Scientific Report SR-001, chapter 13, pages 323–348. European Space Agency, July 1998.
28. C.T. Russell and R.C. Elphic. ISEE observations of flux transfer events at the dayside magnetopause. *Geophys. Res. Lett.*, 6:33–36, 1979.
29. M.A. Saunders, C.T. Russel, and N. Skopke. Flux transfer events: scale size and interior structure. *Geophys. Res. Lett.*, 11:131–134, 1984.
30. S.J. Schwartz. Shock and discontinuity normals, Mach numbers and related parameters. In G. Paschman and P. Daly, editors, *Analysis Methods for Multi-Spacecraft Data*, ISSI Scientific Report SR-001, chapter 10, pages 249–270. European Space Agency, July 1998.
31. D.G. Sibeck. A model for the transient magnetospheric response to sudden solar wind dynamic pressure variations. *J. Geophys. Res.*, 95 (A4):3755–3771, 1990.
32. D.J. Southwood. The ionospheric signature of flux transfer event. *J. Geophys. Res.*, 92:3207–3213, 1987.
33. N. A. Tsyganenko. Global quantitative models of the geomagnetic field in the cis-lunar magnetosphere for different disturbance levels. *pps*, 35:1347–1359, 1987.